Assembly of Graphene Sheets into Hierarchical Structures for High-Performance Energy Storage

Shengyan Yin,[†] Yanyan Zhang,[†] Junhua Kong,[†] Changji Zou,[†] Chang Ming Li,[‡] Xuehong Lu,[†] Jan Ma,[†] Freddy Yin Chiang Boey,[†] and Xiaodong Chen[†,*]

[†]School of Materials Science and Engineering, Nanyang Technological University, 50 Nanyang Avenue, Singapore, 639798, and [‡]School of Chemical and Biomedical Engineering, Nanyang Technological University, 70 Nanyang Drive, Singapore, 637457

ABSTRACT The electrodes with the hierarchical nanoarchitectures could offer a huge increase in energy storage capacity. However, the ability to achieve such hierarchical architectures on a multiple scale still has remained a great challenge. In this paper, we report a scalable self-assembly strategy to create bioinspired hierarchical structures composed of functionalized graphene sheets to work as anodes of lithium-ion batteries. The resulting electrodes with novel multilevel architectures simultaneously optimize ion transport and capacity, leading to a high performance of reversible capacity of up to 1600 mAh/g, and 1150 mAh/g after 50 cycles. Importantly, the process to fabricate such hierarchical structures is facile, low-cost, green, and scalable, providing a universal approach for the rational design and engineering of electrode materials with enhanced performance, and it may have utility in various applications, including biological scaffold, catalysis, and sensors.

KEYWORDS: bioinspiration · hierarchical structures · graphene · self-assembly · lithium-ion battery

A remarkable feature of naturally occurring materials is their hierarchical constructions with a finely carved appearance, such as the porous silica exoskeleton observed in diatoms[1] and natural honeycombs.[2] Such hierarchical constructions on a scale ranging from nanometers to millimeters are characteristic of biological structures, introducing the capability to meet the physical or chemical demands occurring at these different levels. This kind of complex hierarchical structure of natural materials has inspired the materials scientists to develop new types of high-performance engineering materials.[3] Recently, the research and development of high performance energy storage devices, such as batteries and supercapacitors, has drawn much attention since it is essential to meeting continuous energy demands.[4] To enhance the device performance, including energy capacity, power density, and recharge time, it is essential to be able to effectively control the electrode nanostructures, which would also help to uncover the underlying principles that govern the operation, performance limitations, and failure of the devices.[5−8] From these points, natural honeycombs with unattainable improvement in stiffness, strength, toughness, and thermal stability serve as a prototype of truly biomimetic cellular materials.[2] For instance, honeycomb structured panels have been widely used for aircraft design, vehicle technology, and other lightweight constructions due to these decisive advantages.

Graphene, a kind of two-dimensional (2D) nanostructured sp^2 carbon material, has fascinating electronic and mechanical properties due to its unique structure and is therefore highly promising for various applications in nanoelectronics and energy storage/conversion, composites, and other applications.[9−14] Although previous efforts have demonstrated that graphene-based nanosheets could be assembled into 2D thin films or three-dimensional (3D) structures,[12,15] the unique performance based on such assemblies is less addressed. Because of exceptional electrical and mechanical properties, high surface-to-volume ratio, and chemical stability,[16] graphene is a promising electrode material for lithium-ion batteries,[17,18] which have a large initial discharge capacity (600−2042 mAh/g) and reversible capacity (540−1264 mAh/g).[19−22] However, lithium-ion batteries store and release electrical energy by the insertion and extraction of lithium ions through the electrode materials, where the surface area and the surface reaction are important.[4,7] From this point, if we build a hierarchical structured assembly of graphene to work as electrodes for lithium-ion batteries, the large contact area between the electrode and electrolyte has advantages in good cycling performance and short path length for Li-transport, which allow us to maximize

* Address correspondence to chenxd@ntu.edu.sg.

Received for review January 17, 2011 and accepted April 21, 2011.

Published online April 21, 2011
10.1021/nn2001728

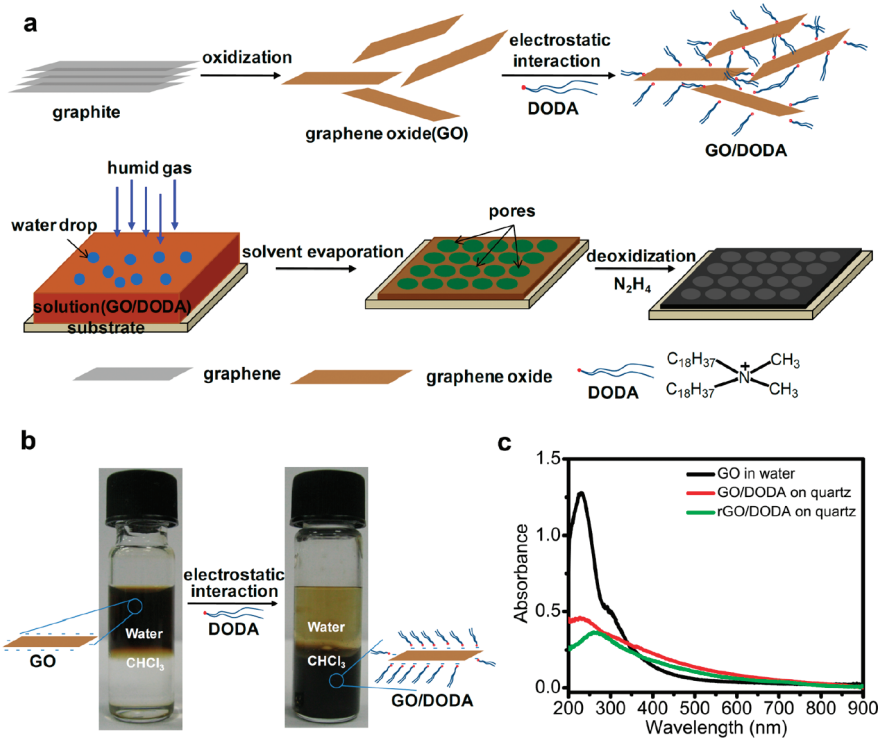

Figure 1. Processes to form honeycomb structures composed of graphene sheets: (a) schematic drawing of the preparation of the honeycomb structured film based on graphene oxide; (b) photographs of the GO solution during phase transfer process by DODA; (c) The UV−vis spectra of the GO in water (black), GO/DODA casting film (red), and the rGO/DODA film after exposure to N_2H_4 vapor (green).

the potential of graphene for applications in energy storage.

In this article, we report a scalable self-assembly strategy to create bioinspired hierarchical structures composed of functionalized graphene sheets. The formed films show high conductivity, high porosity, and robust chemical and mechanical stability. The hierarchical graphene films own novel multilevel architectures, from nanosheets, nanopores, to three-dimensional microscaled porous structures with interconnected active and passive components, which simultaneously optimize ion transport and capacity, leading to a high performance of reversible capacity of up to 1600 mAh/g. Importantly, the process to fabricate such hierarchical structures is facile, low-cost, green, and scalable, providing a universal approach and new opportunities for the rational design and engineering of electrode materials with enhanced performance.

RESULTS AND DISCUSSION

The principle for assembly of graphene sheets into bioinspired honeycomb structures is based on the "breath figure" method,[23,24] as shown in Figure 1a. First, water-soluble graphene oxide (GO) was prepared by oxidizing graphite *via* a modified Hummers method.[25] A prerequisite to use the "breath figure" method to form honeycomb structures is that the GO has to be in the organic phase, but the heavily oxygenated GO is hydrophilic. Therefore, cationic surfactants, such as dimethyldioctadecylammonium bromide (DODA·Br), were chosen to electrostatically adsorb and self-assemble onto the surface of the highly negatively charged GO[26] to form a GO/DODA complex in the organic media such as chloroform, dichloromethane, benzene, and so forth. Another reason to choose DODA·Br is that it has two long alkyl chains (~2.8 nm), which would be able to ensure that the GO/DODA complex was soluble in the organic media and also to prevent the adjacent graphene layers from aggregation when the GO was reduced to graphene. It was obvious that the color of the GO aqueous solution changes from dark brown to light yellow after DODA·Br was added and the chloroform solution color changes to dark brown (Figure 1b), which implies that the hydrophilic surfaces of GO have been modified by the hydrophobic alkyl chains of surfactants and successfully transferred to the organic phase. In addition, height profiles of the single-layer GO AFM images clearly show that the GO surface was modified by DODA layers (Supporting Information, Figure S1). Furthermore, the absorption properties of GO do not change after the addition of DODA, as demonstrated by UV−vis measurement (Figure 1c). The GO has a characteristic peak at 230 nm ($\pi-\pi^*$ transitions of carbon−carbon bonds) and a shoulder at 298 nm (n−π^* transitions of carboxyl bonds).[13,27] The GO/DODA cast film on the quartz exhibited a nearly

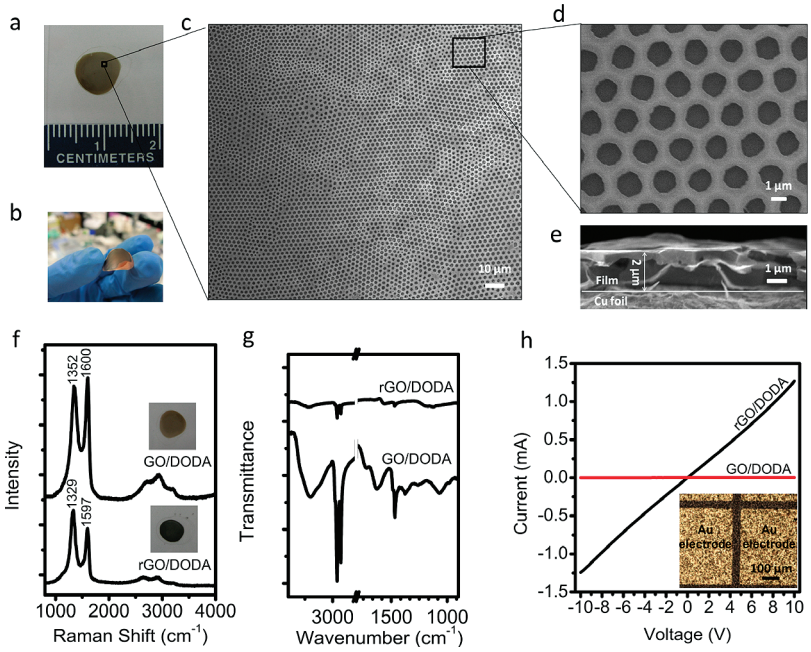

Figure 2. Configuration of the honeycomb structures: (a) photograph of the honeycomb film on the glass; (b) photograph of the honeycomb-patterned film on the copper foil; (c,d) SEM images of honeycomb-patterned film prepared from 1 mg/mL of the GO/DODA complex on the silicon wafer; (e) cross-sectional SEM image of the honeycomb-patterned film on the copper foil; (f) Raman spectra of the GO/DODA (top) and rGO/DODA (bottom) under the 488 nm laser excitation (inset, the photographs of the honeycomb films before and after exposure to N_2H_4 vapor); (g) FT-IR spectral of the rGO/DODA (top) and GO/DODA (bottom); (h) *I*−*V* curve for honeycomb film before and after reduction (inset, the microscopy image of the device for conductivity measurement).

identical absorption peak in comparison to that of native GO in aqueous solution.

Then, the GO/DODA chloroform solution (1 mg/mL) was cast onto glass substrates under a moist airflow (85% relative humidity) applied to the solution surface[24,28,29] to form the honeycomb film, as shown in Figure 1a. After 30−60 s, the solvent and water were evaporated completely and the ordered honeycomb films (Figure 2a,c) were obtained. These films exhibited bright iridescent colors when viewed with reflected light, indicating a periodic refractive index of variation throughout the thickness of the film. The average size of the honeycomb holes was about 1.5 μm (Figure 2d) and the thickness of the film was about 2 μm (Figure 2e). It was noted that there was no honeycomb structures formation when the relative humidity was less than 30%. The reason for this was that the porous structure was templated by the water droplets condensed on the surface of the evaporating solution. It should also be noted that the variation in humidity did not affect the porous structure of the film once the structures were formed.

After that, the N_2H_4 vapor[13,30,31] was used to deoxidize the GO/DODA honeycomb film to the reduced (rGO/DODA) honeycomb film, while the honeycomb structures were kept. Different spectroscopy measurements were used to confirm the formation of rGO in the honeycomb films. The characteristic peak at 230 nm shifted to 264 nm (Figure 1c), which implied that the GO sheets in the composite films were reduced to more conjugated electronic graphene sheets (rGO) after exposure to N_2H_4 vapor.[27] Furthermore, characteristic G and D bands of Raman spectra for the films before and after exposure to N_2H_4 vapor clearly indicated the formation of rGO in the honeycomb films. The G band arose from the zone center E_{2g} mode, corresponding to ordered sp^2 bonded carbon, whereas the D band is ascribed to edges, other defects, and disordered carbon.[32−34] The I_D/I_G intensity ratio was an indicator of the disorder degree and average size of the sp^2 domains. For the GO/DODA honeycomb films, there were two prominent peaks at 1600 cm^{-1} and 1352 cm^{-1} (Figure 2f) corresponding to the well documented G and D bands.[32−34] After the reduction, there were still G and D bands (at 1597 and 1329 cm^{-1}, respectively), but the values of I_D/I_G increased in comparison to the GO/DODA film. This strongly suggested that the GO converted to rGO in the honeycomb films after exposure to N_2H_4 vapor. The elimination of oxygen functional group peaks (1721 cm^{-1} due to the C═O stretching, 1418 cm^{-1} due to carboxy C−O, 1237 cm^{-1} due to epoxy C−O, and 1070 cm^{-1} due to alkoxy C−O groups situated at the edges of the GO nanosheets[35,36]) in the FTIR spectra (Figure 2g) for the reduced films supported this argument, while the peaks at 2918 (CH_2 symmetry stretches) and 2850 cm^{-1} (CH_2 antisymmetry stretches) for the reduced films suggested that surfactant molecules were

still encapsulated within the frame of the honeycomb structures and prevented the graphene sheets from congregating together. Finally, the conductivity measurement revealed that the acquired rGO/DODA honeycomb films had an electrical conductivity of ~4.6 S/m. For the electrical conductivity measurement, we deposited Au microelectrode arrays on the honeycomb film by thermal deposition of a 50 nm Au through a copper grid, as shown in the inset of Figure 2h. Then, we can directly measure the *I*–*V* curves of the honeycomb film before and after reduction (Figure 2h) using the probe station. Although the reduced graphene sheets were disordered (Supporting Information, Figure S2) in their distribution within the frame of the honeycomb films, the edge contacts between the reduced graphene sheets still made the whole film conductive, which ensured efficient electron transport for charge and discharge cycles in battery devices. It was noted that the reduced films were no longer soluble in any organic solvent or water. In addition, the honeycomb structures were thermally stable (no obvious change after they were heated to 400 °C, Supporting Information, Figure S3), which is important for the cycle life of the battery devices.

The obtained honeycomb films showed the hierarchical architectures, which are built up by the graphene nanosheets, the nanopores stacked by these graphene nanosheets, and the microscale honeycomb structure. The method to form such bioinspired hierarchical structures is facile, economic, and nontoxic. It was noted there was no limitation for the size of the honeycomb films, which only depended on the volume of the solution and the size of the substrate, and the films could be flexible if the substrate could be bent (Figure 2b). Here, the cationic surfactant served as the directing agent to help create the bioinspired honeycomb structures to solve the incompatibility and aggregation problems of GO within organic media. In addition, it provided passive components (*e.g.*, DODA) interconnected with active components (rGO) within architectures, which was used for lithium-ion storage. The high surface area, disordered graphene sheets, and numerous nanopores would be favorable for the accessibility of the electrolyte, rapid diffusion of the lithium ions, and host uptake. Furthermore, the graphene layers within the structures would facilitate the fast transport of electrons during the charge–discharge processes owing to the high electrical conductivity of graphene. In addition, the disordered dispersed graphene would assist the diffusion of the lithium ion; the mechanism is similar to that of the disordered carbons (in graphite), showing higher specific capacity than ordered graphitic carbons.[18] However, the nanopores are located next to the edges of a neighboring graphene layer, which are not the typical round or foursquare pores, leading to the fact that the N_2 sorption isotherm cannot provide information of the nanopore size distribution here.[37]

In a proof-of-concept experiment, coin cells (2032) with a metallic Li counter electrode were used to evaluate the electrochemical performance of the rGO/DODA honeycomb films on the copper foil. The capacity and cycle performance of rGO/DODA honeycomb electrodes were evaluated by galvanostatic charge–discharge measurements at a current density of 50 mA/g with a potential window from 0.01 to 3.00 V (*versus* Li/Li^+) (Figure 3a,c,d). Typically, it was striking that a large specific capacity of about 3025 mAh/g was achieved, and the reversible capacity was about 1612 mAh/g for the first process. The reversible capacity of the rGO/DODA honeycomb electrodes was about 1300 mAh/g in the initial 25 cycles and 1150 mAh/g after 50 cycles. To our knowledge, these values were the highest ever reported for the pure carbon materials. A large irreversible capacity of ~1400 mAh/g was observed for the honeycomb electrode during the first discharge/charge process (Figure 3c). The reason can be attributed to formation the solid electrolyte interphase (SEI) film at the electrode/electrolyte interface and the reaction of oxygen-containing functional groups on graphene with lithium ions.[17,38–41] The SEI film and the passivating product of the reaction can block the nanopores then reduce the release quantity of lithium ion.[37] The average of the first reversible capacity for coin cells made by different batches of the rGO/DODA honeycomb electrodes was about 1508 mAh/g, and their representative curves of capacity *versus* cycle number for the honeycomb film were shown in Supporting Information, Figure S4. For comparison, we fabricated smooth rGO/DODA films by simply coating GO/DODA chloroform solution onto a substrate with a chemical reduction and tested the capability of lithium storage. It exhibited a high capacity (1957 mAh/g) in the first discharge process, and the reversible capacity was 1076 mAh/g (Figure 3d). After 50 cycles, the reversible capacity was 678 mAh/g, which was lower than the devices fabricated by the rGO/DODA honeycomb electrodes. In addition, the reversible retention capacity (71%) of the honeycomb electrodes after 50 cycles was higher than that (63%) of the smooth film electrodes. In addition, the honeycomb electrode exhibits very good rate capability operated at various current densities between 50 and 300 mA/g. Cycle performance of honeycomb film at different current densities of 50, 150, and 300 mA/g are shown in Supporting Information, Figure S5. At the current densities of 150 and 300 mA/g, the corresponding reversible specific capacity of the honeycomb films can reach ~1400 mAh/g and ~1200 mAh/g, respectively, indicating that the honeycomb electrodes possess a high rate of discharge/charge capability. From the cycle performance, at the current density of 300 mA/g, a high capacity can still be maintained.

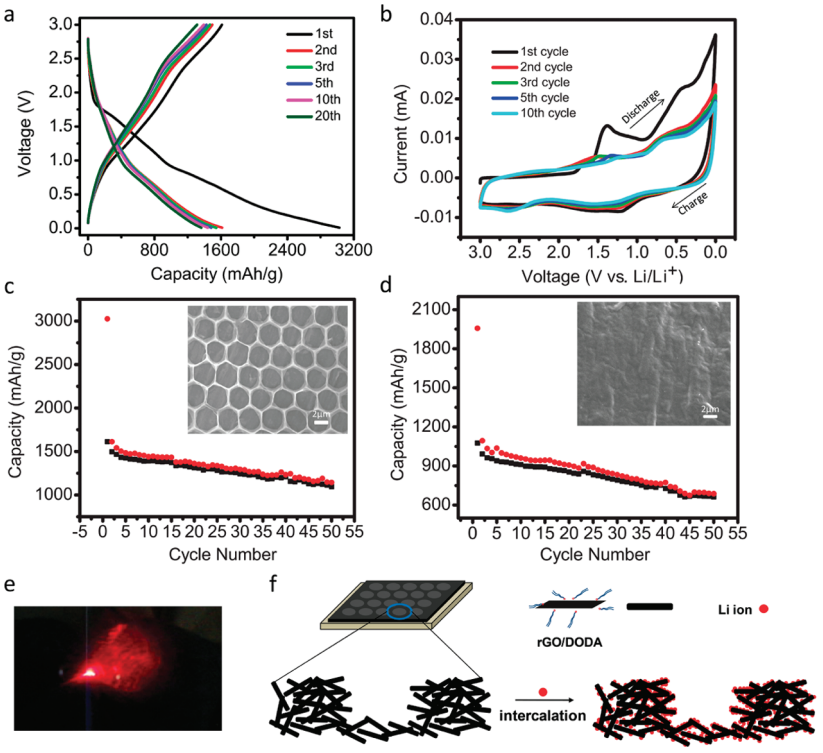

Figure 3. Electrochemical properties of the honeycomb structures: (a) charge and discharge cycle curves of the honeycomb-patterned film as anode in lithium cells at a current density of 50 mA/g; (b) cyclic voltammetry (CV) curves of the honeycomb film (*vs* Li/Li^+ at a scanning rate of 0.1 mV/s); (c,d) capacity *versus* cycle number for the honeycomb film and nonpatterned film at a current density of 50 mA/g showing charge (square, black) and discharge (circle, red) (the insets are the corresponding SEM images); (e) coin cell (2032) used to power a laser pen; (f) possible "falling cards" structure of the honeycomb pores in the lithium ion intercalation.

These results demonstrated that the prepared honeycomb electrodes have an intensive potential as a candidate of anode materials with high reversible capacity, good cycle performance, and high rate discharge/charge capability.[18] Cyclic voltammetry (CV) experiments were further conducted to evaluate the electrochemical performance of the rGO/DODA electrode at a scanning rate of 0.1 mV/s over the voltage range of 0.01−3.00 V (Figure 3b). Two reduction peaks in the potential range of 0.9−1.7 V and 0.3−0.6 V were clearly observed in the first cycle but disappeared during the second cycle. The peak at 0.9−1.7 V may correspond to the irreversible reactions between the honeycomb electrode and Li ions or electrolytes, and the peak at 0.3−0.6 V was due to the cointercalation of the solvated lithium ion into graphene sheets.[42−44] The CV behavior of the rGO/DODA honeycomb structures confirmed that rGO sheets were electrochemically active components for lithium storage. The change from the first cycle to the second cycle may be due to the incomplete conversion reaction and irreversible lithium loss due to the formation of the SEI film, which was supported by the initial capacity loss (about 1400 mAh/g) and the low Coulombic efficiency (about 53%). During the second to the tenth cycle, there was no clear change implying that the electrode was stable during the following charge/discharge cycles after the first cycle. To demonstrate a practical device based on such rGO/DODA honeycomb structures, a coin cell (2032) was used to repeatedly power a laser pen, as shown in Figure 3e.

There are two possible reasons for the observed high capacity of rGO/DODA hierarchical films which was unprecedented for pure carbon materials. One reason is the disordered reduced graphene sheets in the honeycomb structure. It would then be easy for lithium ions, electrochemically adsorbed on both sides of single-layer sheets, edges, and other defects,[17] to have high reversible storage capability. As reported by others,[20] the film made by disordered graphene nanosheets showed the greatly enhanced capacity (~1054 mAh/g) which is similar to the capacity (~1000 mAh/g) of the rGO/DODA smooth film in this work. Another reason is because of the higher surface-to-volume ratio in hierarchical structures. The large contact area between the electrode and electrolyte would then have advantages in good cycling performance and short path length for Li-transport.[38,45] The reduced graphene oxide sheets were arranged like "falling cards" (Figure 3f).[17,46] The diffusion distance of the lithium ions into the host position would affect the capacity of the lithium-ion battery. In this work, we used the surfactant to encapsulate each graphene

sheet, which not only increased the distance between two graphene sheets, but also helped to form the porous structure. The nanopores between the graphene sheets allowed for efficient anode performance. If the path of Li ions was blocked or impeded in a narrow channel, the interconnected porous network within honeycomb frame would allow for the redirection of the ion traffic, maintaining a rapid charging capability. The longer distance between the graphene layers and the bigger surface area made it easier for the lithium ions to reach the position. Also, the honeycomb microstructures provided extra space for the electrolyte accommodation,[17,47] and these properties may facilitate electrolyte contact as well as ionic diffusion and thereby result in a large capacity and favorable rate performance. The hierarchical graphene films own novel multilevel architectures, from nanosheets and nanopores, to three-dimensional microscopic porous structures with interconnected active and passive components, which simultaneously optimize ion transport and capacity, leading to a high performance of reversible capacity of up to 1600 mAh/g. However, it is noted that nanostructures having a large surface area not only benefit the reactivity but also decrease the tap density of the electrode. One inherent disadvantage of porous structures is the low volumetric energy density. To enhance the volumetric energy density, the 3D concept can be extended.[7] Actually, 3D cavities and nanopores would also contribute to the lithium storage, where lithium is intercalated in graphene layers and lithium is stored in cavities.[7,48]

CONCLUSIONS

We successfully assembled the graphene sheets into bioinspired honeycomb structures through the control of chemistry and assembly processes. The rGO honeycomb structured films that were obtained showed high conductivity, high porosity, and robust chemical and mechanical stability, which lead to a high performance energy–storage device. The honeycomb graphene electrode exhibited a large reversible capacity (1150 mAh/g after 50 cycles) and an excellent cyclic performance, highlighting the advantages of bioinspired hierarchical structures for energy storage applications in high-performance lithium-ion batteries. Porosity was important for improving the capacity and cycling performance of disordered carbon anode materials, since the porous framework could significantly decrease the diffusion distance of the lithium ions into the disordered graphene layers, which can enhance the charge/discharge rate performance of rechargeable lithium batteries. Finally, the fabrication process of such hierarchical structured graphene films was simple, low-cost, green, and scalable, which not only provides new opportunities for the rational design and engineering of electrode materials with enhanced performance, but also may find utility in various applications, including biological scaffold, catalysis, and sensors.

METHODS

Preparation of Graphite Oxide. Graphite oxide was prepared from natural graphite powder (Sigma, 45 μm) *via* a modified Hummers method.[13,25,30,49] Typically, graphite powder (0.3 g) was put into an 80 °C solution of concentrated H_2SO_4 (2.4 mL), $K_2S_2O_8$ (0.5 g), and P_2O_5 (0.5 g). The mixture was kept at 80 °C for 4 h and then cooled to room temperature, diluted with deionized water (DI, 0.5 L), and then filtrated. The powder produced was preoxidized product. The preoxidized graphite was further oxidized in concentrated H_2SO_4 (12 mL) and $KMnO_4$ (1.5 g). After the addition of $KMnO_4$, the mixture was stirred at 35 °C for 2 h. Then, the mixture was diluted with DI water (25 mL) in an ice bath to keep the temperature below 50 °C. After it was stirred for 2 h, it was further diluted with DI water (70 mL). Then 30% H_2O_2 (2 mL) was added to the mixture, and a brilliant yellow product was formed. The product was filtrated and washed with HCl aqueous solution (1:10, 1 L) and DI water (1 L). Purified graphite oxide suspensions were then dispersed in water to create a 0.1 wt % dispersion. Exfoliation of graphite oxide was achieved by ultrasonication for 2 h. The obtained brown dispersion was then subjected to 30 min of centrifugation at 3000 rpm to remove any unexfoliated graphite oxide (usually present in a very small amount), using a themo-centrifuge with a rotor radius of 14 cm.

Preparation of the Composite Material. Following the method reported in literature,[26] we prepared the composite material. The above graphene oxide (GO) solution was subjected to another 30 min of centrifugation at 14000 rpm. We then adjusted the pH value of the top clean solution to about 9 with 1 mol/L NaOH aqueous solution. After that, we titrated the GO aqueous solution with 1 mg/mL DODA·Br chloroform solution. When the color of aqueous solution changed to light yellow (Figure 1b), we stopped adding DODA·Br chloroform solution. The organic phase was then separated and washed by DI water. Finally, the composite material GO/DODA was obtained by evaporating the chloroform to dryness.

Preparation of the Honeycomb Films. Typically, the honeycomb thin films were prepared by direct casting GO/DODA complex chloroform solution (1 mg/mL) onto the glass substrates under a moist airflow (relative humidity *ca.* 85%). The brown thin films covering an area of *ca.* 2 cm^2 were left behind after the complete evaporation of the solvent and water within 30–60 s. Following the same process, we would get such honeycomb films on the different substrates, such as silicon wafer and copper foil. The control experiments without humid airflow had been performed in the desiccators (relative humidity *ca.* 30%) and no macroporous structures developed, leaving only unpatterned flat films as a result. To keep the macroporous structure, we used the hydrazine vapor to reduce the film. The films were then put into the autoclave, and then 10 μL of hydrazine monohydrate was added into the autoclave. Finally, the autoclave was heated at 90 °C for 16 h to get the reduced films. The current–voltage characteristics of the films were obtained using a probe station (Lakeshore CRX-4K, Westerville, OH, USA) for connecting the microelectrodes, combined with semiconductor parameter analyzer (Keithley 4200-SCS, Cleveland, OH, USA) for application of potential and measurement of current.

Electrochemical Measurements. The film used to do electrochemical measurements was built on the copper foil directly. Electrochemical evaluation was done using 2032 coin cells hardware. Half cells were then assembled in a Ar-filled drybox

(<1 ppm H_2O/O_2) using Li metal foils as counter electrodes and Celgard Septum separators saturated with 1 M LiPF6 in 1:1 ethylene carbonate/dimethyl carbonate (EC/DMC, Ferro Corp). The charge/discharge tests were performed using a battery analyzer (MTI) at the current density of 50 mA/g with a voltage window of 0.01−3.00 V. Cyclic voltammetry (CV) curves were measured at 0.1 mV/s within the range of 0.01−3.00 V using an electrochemistry workstation (CHI, 660D).

Acknowledgment. This work was supported by National Research Foundation of Singapore (NRF-RF2009-04 and CREATE).

Supporting Information Available: AFM data, TEM images of the honeycomb film, SEM image after heated treatment, cycle performance of honeycomb electrode at different current densities, and representative curves of capacity *versus* cycle number for the different honeycomb films. This material is available free of charge *via* the Internet at http://pubs.acs.org.

REFERENCES AND NOTES

1. Sanchez, C.; Arribart, H.; Guille, M. M. G. Biomimetism and Bioinspiration As Tools for The Design of Innovative Materials and Systems. *Nat. Mater.* **2005**, *4*, 277–288.
2. Zhang, K.; Duan, H.; Karihaloo, B. L.; Wang, J. Hierarchical, Multilayered Cell Walls Reinforced by Recycled Silk Cocoons Enhance The Structural Integrity of Honeybee Combs. *Proc. Natl. Acad. Sci.U.S.A.* **2010**, *107*, 9502–9506.
3. Fratzl, P.; Barth, F. G. Biomaterial Systems for Mechanosensing and Actuation. *Nature* **2009**, *462*, 442–448.
4. Armand, M.; Tarascon, J. M. Building Better Batteries. *Nature* **2008**, *451*, 652–657.
5. Arico, A. S.; Bruce, P.; Scrosati, B.; Tarascon, J. M.; Van Schalkwijk, W. Nanostructured Materials for Advanced Energy Conversion and Storage Devices. *Nat. Mater.* **2005**, *4*, 366–377.
6. Guo, Y.-G.; Hu, J.-S.; Wan, L.-J. Nanostructured Materials for Electrochemical Energy Conversion and Storage Devices. *Adv. Mater.* **2008**, *20*, 2878–2887.
7. Bruce, P. G.; Scrosati, B.; Tarascon, J.-M. Nanomaterials for Rechargeable Lithium Batteries. *Angew. Chem., Int. Ed.* **2008**, *47*, 2930–2946.
8. Maier, J. Nanoionics: Ion Transport and Electrochemical Storage in Confined Systems. *Nat. Mater.* **2005**, *4*, 805–815.
9. Geim, A. K.; Novoselov, K. S. The Rise of Graphene. *Nat. Mater.* **2007**, *6*, 183–191.
10. Dreyer, D. R.; Park, S.; Bielawski, C. W.; Ruoff, R. S. The Chemistry of Graphene Oxide. *Chem. Soc. Rev.* **2010**, *39*, 228–240.
11. Stankovich, S.; Dikin, D. A.; Dommett, G. H. B.; Kohlhaas, K. M.; Zimney, E. J.; Stach, E. A.; Piner, R. D.; Nguyen, S. T.; Ruoff, R. S. Graphene-Based Composite Materials. *Nature* **2006**, *442*, 282–286.
12. Lee, S. H.; Kim, H. W.; Hwang, J. O.; Lee, W. J.; Kwon, J.; Bielawski, C. W.; Ruoff, R. S.; Kim, S. O. Three-Dimensional Self-Assembly of Graphene Oxide Platelets into Mechanically Flexible Macroporous Carbon Films. *Angew. Chem., Int. Ed.* **2010**, *49*, 10084–10088.
13. Li, D.; Muller, M. B.; Gilje, S.; Kaner, R. B.; Wallace, G. G. Processable Aqueous Dispersions of Graphene Nanosheets. *Nat. Nanotechnol.* **2008**, *3*, 101–105.
14. Zhu, Y.; Murali, S.; Cai, W.; Li, X.; Suk, J. W.; Potts, J. R.; Ruoff, R. S. Graphene and Graphene Oxide: Synthesis, Properties, and Applications. *Adv. Mater.* **2010**, *22*, 3906–3924.
15. Cote, L. J.; Kim, F.; Huang, J. Langmuir−Blodgett Assembly of Graphite Oxide Single Layers. *J. Am. Chem. Soc.* **2008**, *131*, 1043–1049.
16. Geim, A. K. Graphene: Status and Prospects. *Science* **2009**, *324*, 1530–1534.
17. Kaskhedikar, N. A.; Maier, J. Lithium Storage in Carbon Nanostructures. *Adv. Mater.* **2009**, *21*, 2664–2680.
18. Liang, M.; Zhi, L. Graphene-Based Electrode Materials for Rechargeable Lithium Batteries. *J. Mater. Chem.* **2009**, *19*, 5871–5878.
19. Yoo, E.; Kim, J.; Hosono, E.; Zhou, H.-S.; Kudo, T.; Honma, I. Large Reversible Li Storage of Graphene Nanosheet Families for Use in Rechargeable Lithium Ion Batteries. *Nano Lett.* **2008**, *8*, 2277–2282.
20. Pan, D.; Wang, S.; Zhao, B.; Wu, M.; Zhang, H.; Wang, Y.; Jiao, Z. Li Storage Properties of Disordered Graphene Nanosheets. *Chem. Mater.* **2009**, *21*, 3136–3142.
21. Wang, G.; Shen, X.; Yao, J.; Park, J. Graphene Nanosheets for Enhanced Lithium Storage in Lithium Ion Batteries. *Carbon* **2009**, *47*, 2049–2053.
22. Yang, S. B.; Feng, X. L.; Wang, L.; Tang, K.; Maier, J.; Mullen, K. Graphene-Based Nanosheets with a Sandwich Structure. *Angew. Chem., Int. Ed.* **2010**, *49*, 4795–4799.
23. François, B.; Pitois, O.; François, J. Polymer Films with a Self-Organized Honeycomb Morphology. *Adv. Mater.* **1995**, *7*, 1041–1044.
24. Widawski, G.; Rawiso, M.; Francois, B. Self-Organized Honeycomb Morphology of Star-Polymer Polystyrene Films. *Nature* **1994**, *369*, 387–389.
25. Hummers, W. S.; Offeman, R. E. Preparation of Graphitic Oxide. *J. Am. Chem. Soc.* **1958**, *80*, 1339–1339.
26. Liang, Y.; Wu, D.; Feng, X.; Müllen, K. Dispersion of Graphene Sheets in Organic Solvent Supported by Ionic Interactions. *Adv. Mater.* **2009**, *21*, 1679–1683.
27. Yang, Q.; Pan, X.; Huang, F.; Li, K. Fabrication of High-Concentration and Stable Aqueous Suspensions of Graphene Nanosheets by Noncovalent Functionalization with Lignin and Cellulose Derivatives. *J. Phy. Chem. C* **2010**, *114*, 3811–3816.
28. Bu, W.; Li, H.; Sun, H.; Yin, S.; Wu, L. Polyoxometalate-Based Vesicle and Its Honeycomb Architectures on Solid Surfaces. *J. Am. Chem. Soc.* **2005**, *127*, 8016–8017.
29. Srinivasarao, M.; Collings, D.; Philips, A.; Patel, S. Three-Dimensionally Ordered Array of Air Bubbles in a Polymer Film. *Science* **2001**, *292*, 79–83.
30. Kovtyukhova, N. I.; Ollivier, P. J.; Martin, B. R.; Mallouk, T. E.; Chizhik, S. A.; Buzaneva, E. V.; Gorchinskiy, A. D. Layer-by-Layer Assembly of Ultrathin Composite Films From Micron-Sized Graphite Oxide Sheets and Polycations. *Chem. Mater.* **1999**, *11*, 771–778.
31. Tung, V. C.; Allen, M. J.; Yang, Y.; Kaner, R. B. High-Throughput Solution Processing of Large-Scale Graphene. *Nat. Nanotechnol.* **2009**, *4*, 25–29.
32. Stankovich, S.; Dikin, D. A.; Piner, R. D.; Kohlhaas, K. A.; Kleinhammes, A.; Jia, Y.; Wu, Y.; Nguyen, S. T.; Ruoff, R. S. Synthesis of Graphene-Based Nanosheets *via* Chemical Reduction of Exfoliated Graphite Oxide. *Carbon* **2007**, *45*, 1558–1565.
33. Shen, J.; Hu, Y.; Li, C.; Qin, C.; Shi, M.; Ye, M. Layer-by-Layer Self-Assembly of Graphene Nanoplatelets. *Langmuir* **2009**, *25*, 6122–6128.
34. Jung, I.; Dikin, D. A.; Piner, R. D.; Ruoff, R. S. Tunable Electrical Conductivity of Individual Graphene Oxide Sheets Reduced at "Low" Temperatures. *Nano Lett.* **2008**, *8*, 4283–4287.
35. Murugan, A. V.; Muraliganth, T.; Manthiram, A. Rapid, Facile Microwave−Solvothermal Synthesis of Graphene Nanosheets and Their Polyaniline Nanocomposites for Energy Storage. *Chem. Mater.* **2009**, *21*, 5004–5006.
36. Park, S.; An, J.; Jung, I.; Piner, R. D.; An, S. J.; Li, X.; Velamakanni, A.; Ruoff, R. S. Colloidal Suspensions of Highly Reduced Graphene Oxide in a Wide Variety of Organic Solvents. *Nano Lett.* **2009**, *9*, 1593–1597.
37. Fukui, H.; Ohsuka, H.; Hino, T.; Kanamura, K. A Si-O-C Composite Anode: High Capability and Proposed Mechanism of Lithium Storage Associated with Microstructural Characteristics. *ACS Appl. Mater. Interfaces* **2010**, *2*, 998–1008.
38. Hu, Y. S.; Adelhelm, P.; Smarsly, B. M.; Hore, S.; Antonietti, M.; Maier, J. Synthesis of Hierarchically Porous Carbon Monoliths with Highly Ordered Microstructure and Their Application in Rechargeable Lithium Batteries with High-Rate Capability. *Adv. Funct. Mater.* **2007**, *17*, 1873–1878.
39. Yang, S.; Feng, X.; Zhi, L.; Cao, Q.; Maier, J.; Müllen, K. Nanographene-Constructed Hollow Carbon Spheres and

Their Favorable Electroactivity with Respect to Lithium Storage. *Adv. Mater.* **2010**, *22*, 838–842.
40. Bhardwaj, T.; Antic, A.; Pavan, B.; Barone, V.; Fahlman, B. D. Enhanced Electrochemical Lithium Storage by Graphene Nanoribbons. *J. Am. Chem. Soc.* **2010**, *132*, 12556–12558.
41. Zhou, G.; Wang, D.-W.; Li, F.; Zhang, L.; Li, N.; Wu, Z.-S.; Wen, L.; Lu, G. Q.; Cheng, H.-M. Graphene-Wrapped Fe_3O_4 Anode Material with Improved Reversible Capacity and Cyclic Stability for Lithium Ion Batteries. *Chem. Mater.* **2010**, *22*, 5306–5313.
42. Pan, Q. M.; Guo, K. K.; Wang, L. Z.; Fang, S. B. Novel Modified Graphite as Anode Material for Lithium Ion Batteries. *J. Mater. Chem.* **2002**, *12*, 1833–1838.
43. Choi, Y.-K.; Chung, K.-i.; Kim, W.-S.; Sung, Y.-E. Electrochemical Properties of Passivation Film on Mesophase Pitch-Based Carbon Fiber Electrode. *Microchem. J.* **2001**, *68*, 61–70.
44. Fan, Z.-J.; Yan, J.; Wei, T.; Ning, G.-Q.; Zhi, L.-J.; Liu, J.-C.; Cao, D.-X.; Wang, G.-L.; Wei, F. Nanographene-Constructed Carbon Nanofibers Grown on Graphene Sheets by Chemical Vapor Deposition: High-Performance Anode Materials for Lithium Ion Batteries. *ACS Nano* **2011**, 10.1021/nn200195k.
45. Magasinski, A.; Dixon, P.; Hertzberg, B.; Kvit, A.; Ayala, J.; Yushin, G. High-Performance Lithium-Ion Anodes Using a Hierarchical Bottom-Up Approach. *Nat. Mater.* **2010**, *9*, 353–358.
46. Zheng, T.; Liu, Y. H.; Fuller, E. W.; Tseng, S.; Vonsacken, U.; Dahn, J. R. Lithium Insertion in High-Capacity Carbonaceous Materials. *J. Electrochem. Soc.* **1995**, *142*, 2581–2590.
47. Wang, Q.; Li, H.; Chen, L.; Huang, X. Monodispersed Hard Carbon Spherules with Uniform Nanopores. *Carbon* **2001**, *39*, 2211–2214.
48. Winter, M.; Besenhard, J. O.; Spahr, M. E.; Novak, P. Insertion Electrode Materials for Rechargeable Lithium Batteries. *Adv. Mater.* **1998**, *10*, 725–763.
49. Park, S.; Ruoff, R. S. Chemical Methods for The Production of Graphenes. *Nat. Nanotechnol.* **2009**, *4*, 217–224.